Electronic Supplementary Material for CrystEngComm

Supporting information for:

Triply interpenetrated (3,4)- and (3,5)-connected binodal metal-organic networks prepared from 1,3,5-benzenetrisbenzoate and 4,4′-bipyridyl

Romain Heck, John Bacsa, John E. Warren, Matthew J. Rosseinsky and Darren Bradshaw*

Additional Structural Representations of 1

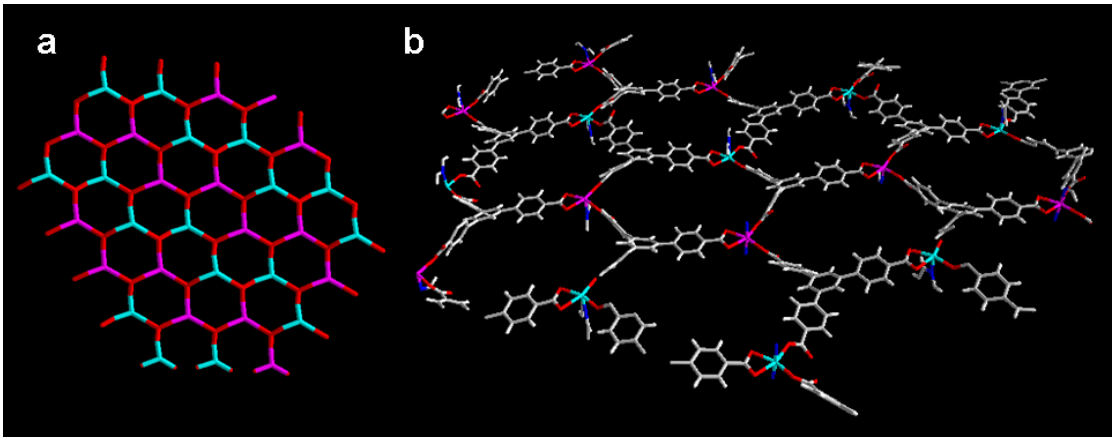

Figure S1. (a) A wire representation of a single (6,3)-type layer of **1** showing the arrangement of the BTB ligands (red) with the two types of Ni centre in the asymmetric unit of **1** (cyan and purple) that act as an additional set of trigonal nodes if only the layer is considered. Each BTB ligand is coordinated to 1xNi(1) and 2xNi(2) or 2xNi(1) and 1xNi(2) (b) The (6,3) layer is non-planar but corrugated in nature due to the significant twisting of the external aromatic rings with respect to the central ring of the BTB ligands. Torsion angles between these rings lie in the range -23.7 to 50.9°. (Ni – cyan/purple, C- grey, H – white, O – red, N – blue; disordered ring components are omitted for clarity)

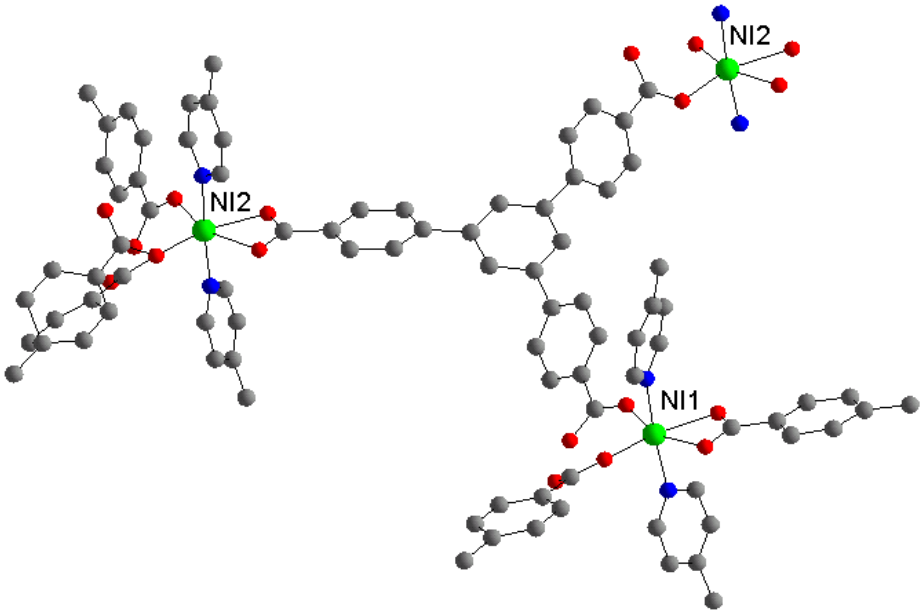

Figure S2. Coordination about Ni(1) and Ni(2) within the layer of **1** showing that the disordered BTB ring, and hence carboxylate donor, is bound only to Ni(2). In this representation the central BTB ligand is bound to 1xNi(1) and 2xNi(2). See S1 figure caption for further information. Hydrogen atoms omitted. (Ni – green, C- grey, O – red, N – blue)

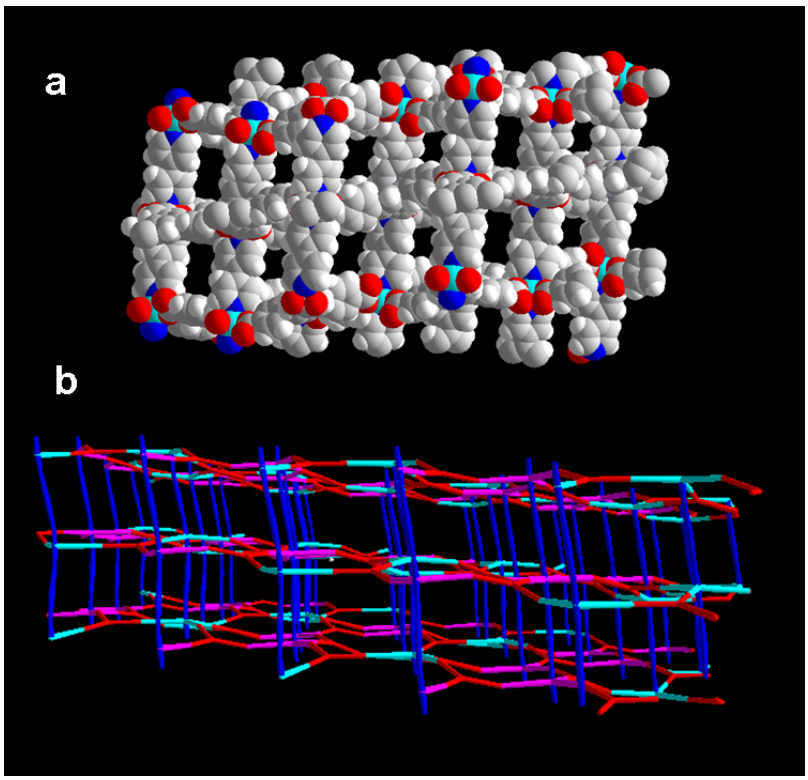

Figure S3. (a) A space filling plot of a single network of **1** perpendicular to the (6,3) layer showing the bipy pillaring groups and the 9 x 10 Å windows they define. (Ni – cyan/purple, C- grey, H – white, O – red, N – blue). (b) The same view showed as a wire representation to highlight the very open structure of the basic network. Colouring as for S1 with bipy pillars shown as blue rods.

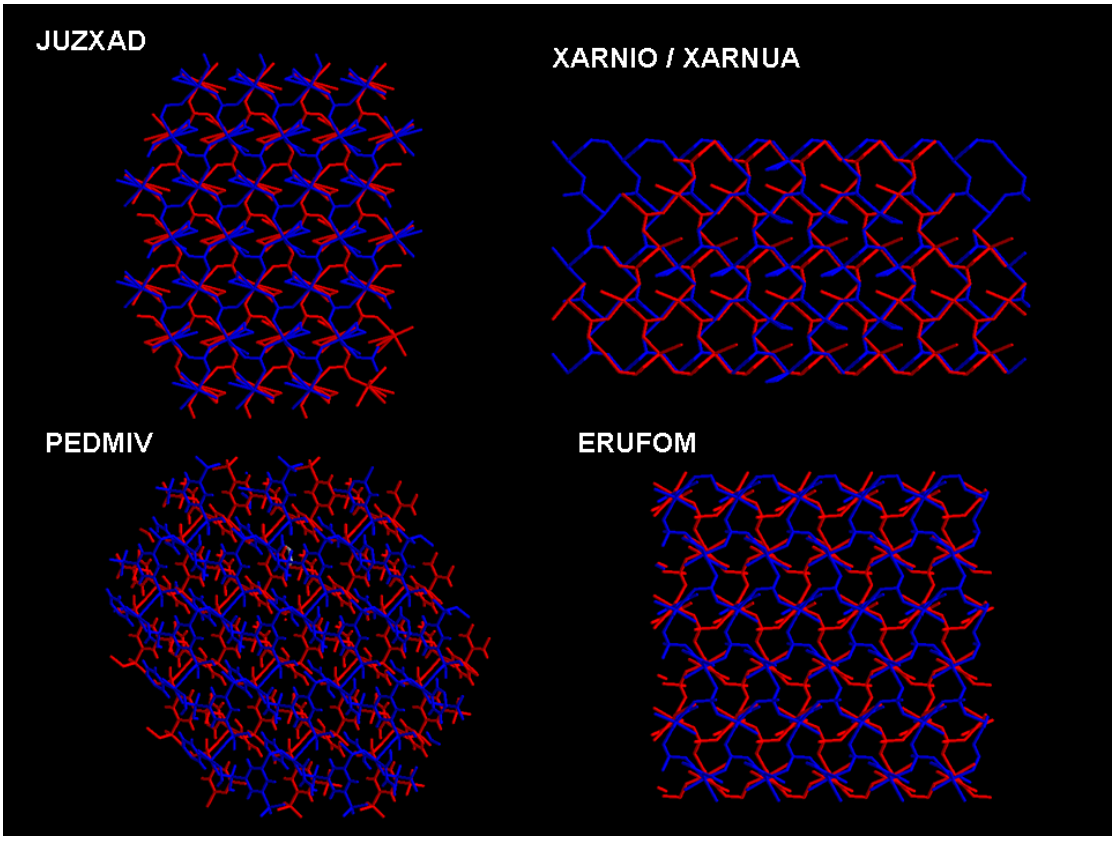

Figure S4. Non-interpenetrated (3,5)-connected metal-organic binodal **gra** networks highlighting the ABA stacking arrangements between layers shown in red and blue in each case. These networks were identified by searching the TOPOS4.0 and RCSR databases. JUZXAD [CuL(H_2O)(SO_4)] · 2(H_2O) where L = 2,5-bis(4-pyridyl)-1,3,4-oxadiazole, *Dalton Trans.* 2003, 1472; ERUFOM [CuL(H_2O)(SO_4)] · 2(H_2O) where L = 2,5-bis(4-pyridyl)-1,3,4-thiadiazole, *Inorg. Chem.* 2004, **43**, 931; PEDMIV [Cu(H4L)(bipy) where L = 1,3,5-benzenetriphosphoric acid, *Inorg. Chem.* 2006, **45**, 977; XARNO [Co(L)(SO_4)] where L = propane-1,3-diamine, XARNUA [Co(L)(SO_4)] where L = pentane-1,5-diamine, *Can. J. Chem*. 2005, **83**, 668.

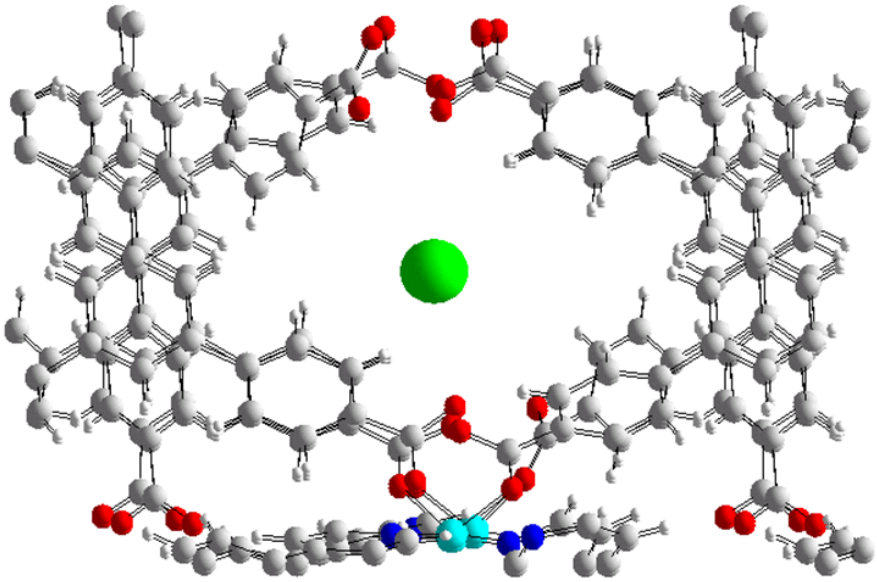

Figure S5. View of a single channel of the triply-interpenetrated structure of **1**. The green sphere marks the centre of the channel and the closest contacts across the windows providing access to the channels are 4.65 x 3.68 Å. The windows are clearly limited by the orientation of the BTB aromatic hydrogen atoms which project into the channel space. Atom colour scheme as for S2.

Bulk characterisation and Properties of 1

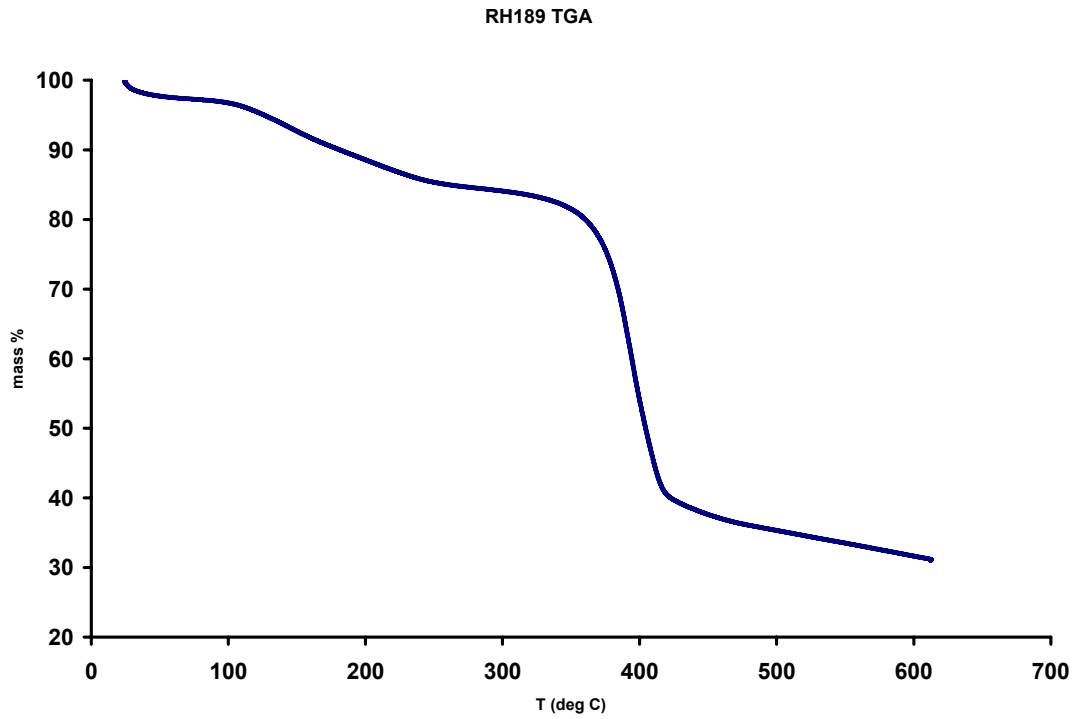

Figure S6. TGA data for **1**. The first mass loss (3.1 %) up to 100°C corresponds to release of guest water molecules and the second loss (10.7 %) to 330°C is for the release of guest DEF. This is in good agreement with the bulk and crystallographically derived formulae.

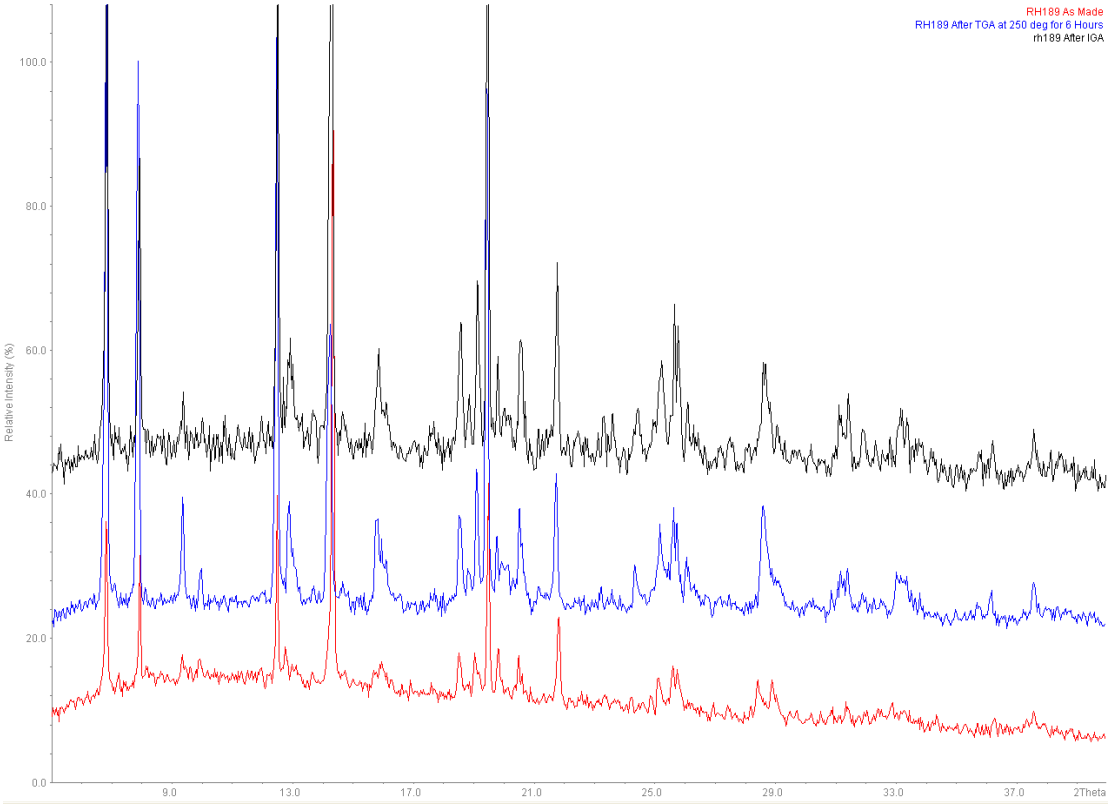

Figure S7. Powder X-ray diffraction data of **1**: as-synthesised (red), after the sample is heated to 250°C in a He flow for 6 hours (blue) and post CO_2 sorption isotherm (black). The samples were sealed in glass capillaries and measured in transmission mode on a Stoe-Stadi P diffractometer using Cu $K_{\alpha 1}$ radiation. Refined cell parameters for the as-made sample: a = 14.4455(17) Å, b = 30.2791(207) Å, c = 16.6388(171) Å, β = 91.690(7)°. Refined parameters for the post-isotherm sample: a = 14.4692(263) Å, b = 30.2408(465) Å, c = 16.5229(239) Å, β = 91.800(13)°.

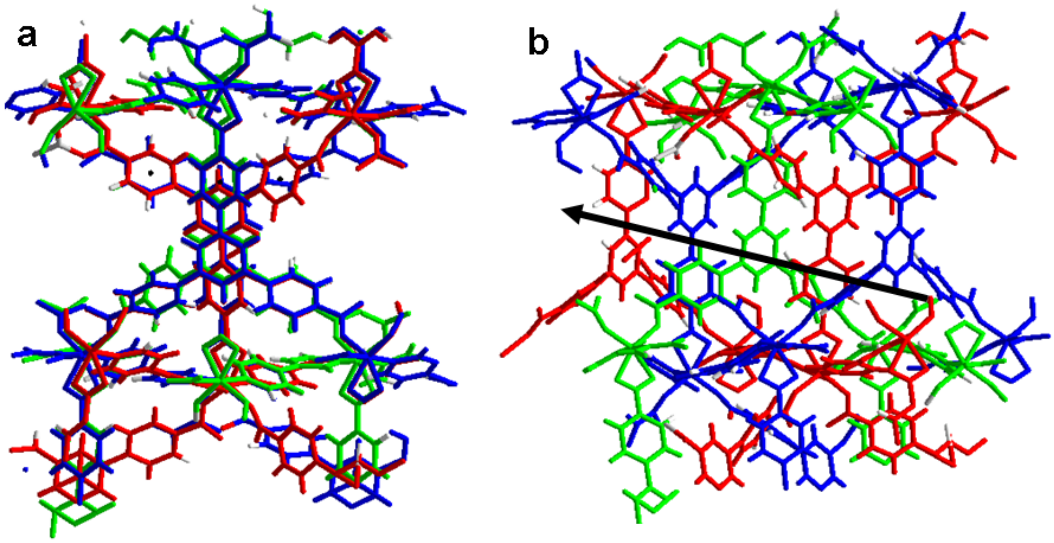

Figure S8. The close inter-network contacts in the triply-interpenetrated structure of **1** viewed (a) along the stacking direction, *c* and (b) perpendicular to this. The contacts between the aromatic rings of the BTB ligands 'stacked' along the black arrow in (b) lie in the range 4.09 – 4.26 Å. Additional contacts also exist between the networks in other parts of the structure. For an additional reference involving 'stacking' of aromatic molecules please see Y. Yamauchi, M. Yoshizawa, M. Fujita, *J. Am. Chem. Soc.* 2008, **130**, 5832-5833

Additional Structural Representations of 2

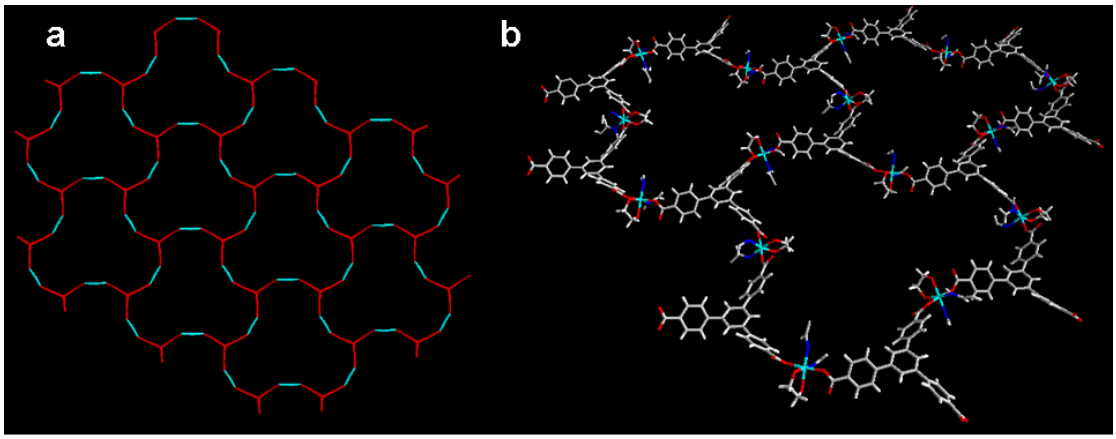

Figure S9. (a) Wire representation of a single (6,3)-type layer in **2**. The Ni centres (cyan) act as linear connectors linking the trigonal BTB nodes (red). (b) Despite the approximately orthogonal arrangement of the *trans* BTB ligands, a layer structure is obtained due to the twisting between the aromatic rings of the BTB ligands. The torsion angle between the central and external aromatic rings is -42°. (Ni – cyan/purple, C- grey, H – white, O – red, N – blue). For further information see figure S10 below.

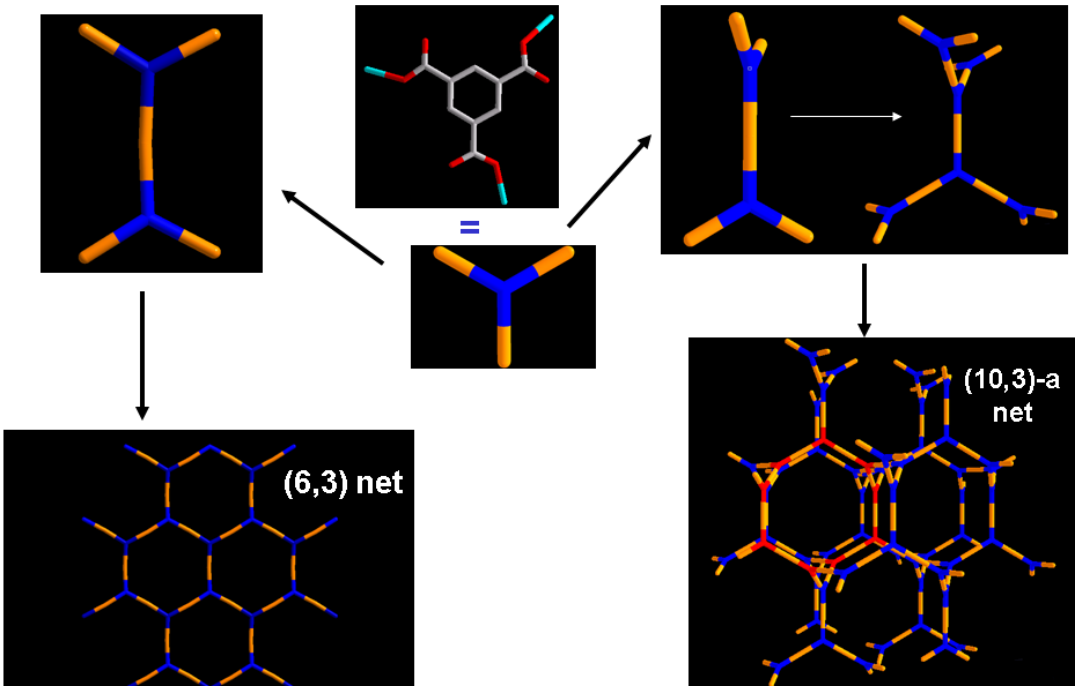

Figure S10. Construction of (6,3) and (10,3)-*a* networks from planar trigonal nodes such as 1,3,5-benzenetricarboxylate (BTC). The BTC nodes (blue) are linearly connected by Ni(II) (orange). When the nodes are bound to the metal in a co-planar arrangement a (6,3) network results. However, when these are locked orthogonal to one another a chiral (10,3)-*a* network propagates.

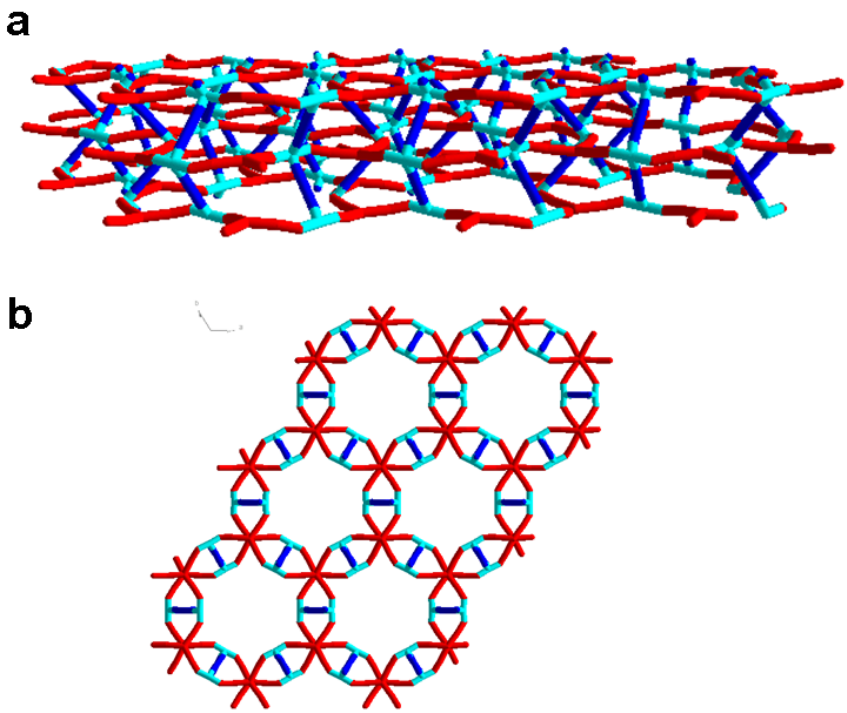

Figure S11. (a) Wire representation of a single network of **2** highlighting the open nature of the structure and the zig-zag Ni-Bipy-Ni chains arising from the cis coordination that pillar the layers. (b) A view parallel to the stacking direction of **2**. (Ni – cyan, BTB – red, bipy – blue)

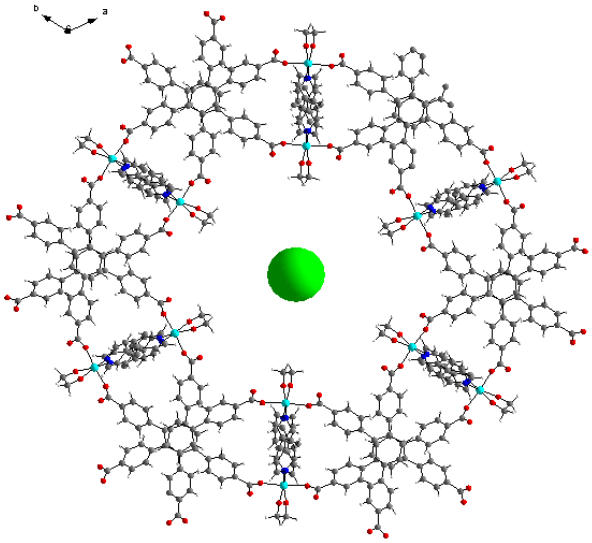

Figure S12. Void centre (green) in a single network of **2**. The window providing access to the void is 11.6 Å across limited by the EG $–CH_2-CH_2-$ groups which project into the pore space. The large voids allow the triple interpenetration of the (3, 4)-connected **tfz** networks.

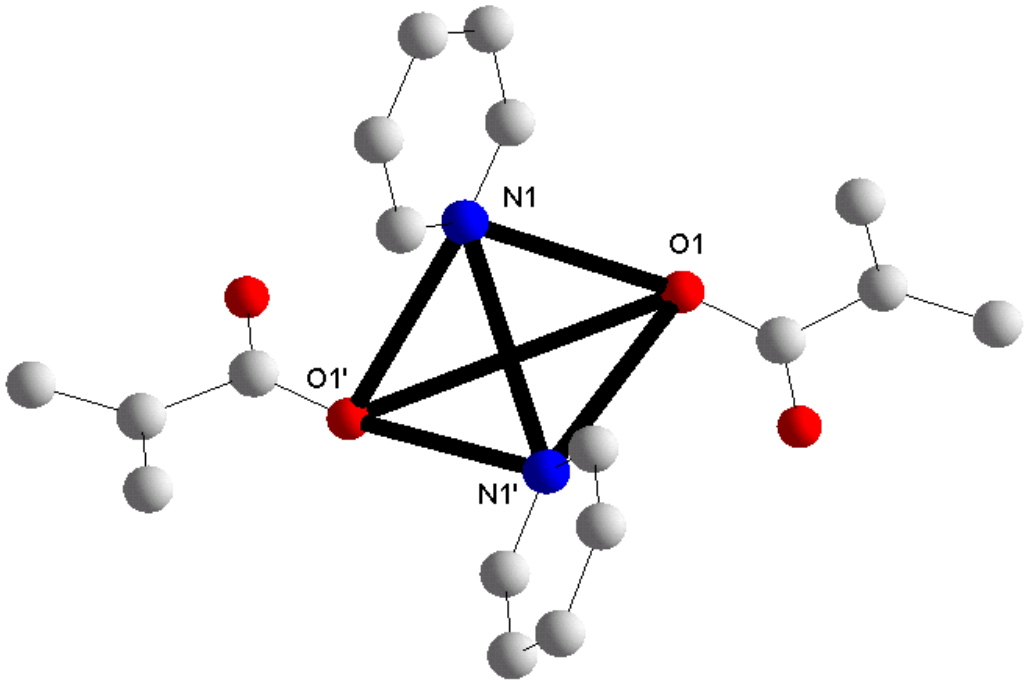

Figure S13. Geometry about the 4-connected Ni(II) node in **2**. The Ni centre (omitted) sits midway along the long vertex between O1-O1'. The distances between the donor atoms that define the vertices of the triangular-based pyramidal node are: O1-N1 (O1'-N1') 2.770(4)Å, O1-N1' (O1'-N1) 2.946(4)Å, N1-N1' 3.139(4)Å, O1-O1' 4.063(3)Å. The long vertex between O1 and O1' is 1.30 – 1.46 times the length of the other 5 vertices. Atoms labelled X' are related by the symmetry operation (0.3333+x-y, 0.6667-y, 0.1667-z). Bipy and BTB ligands are only partially shown for clarity.

Bulk characterisation and Properties of 2

(a)

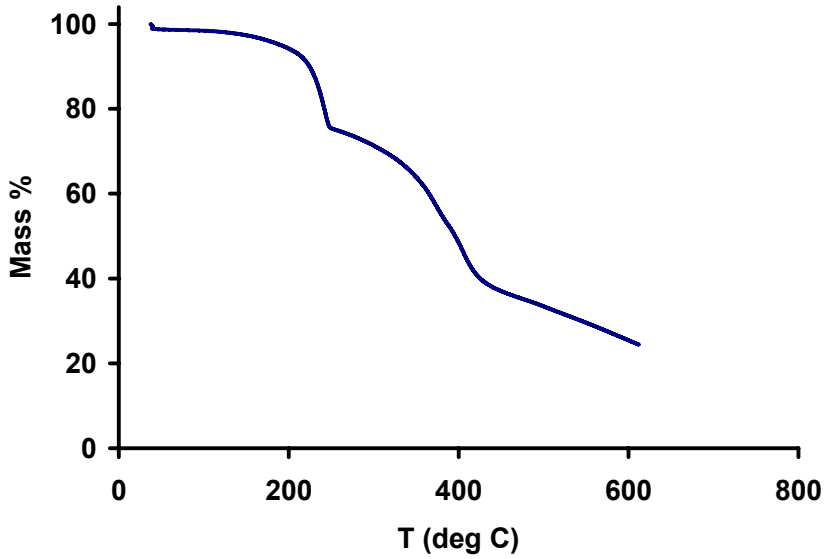

(b)

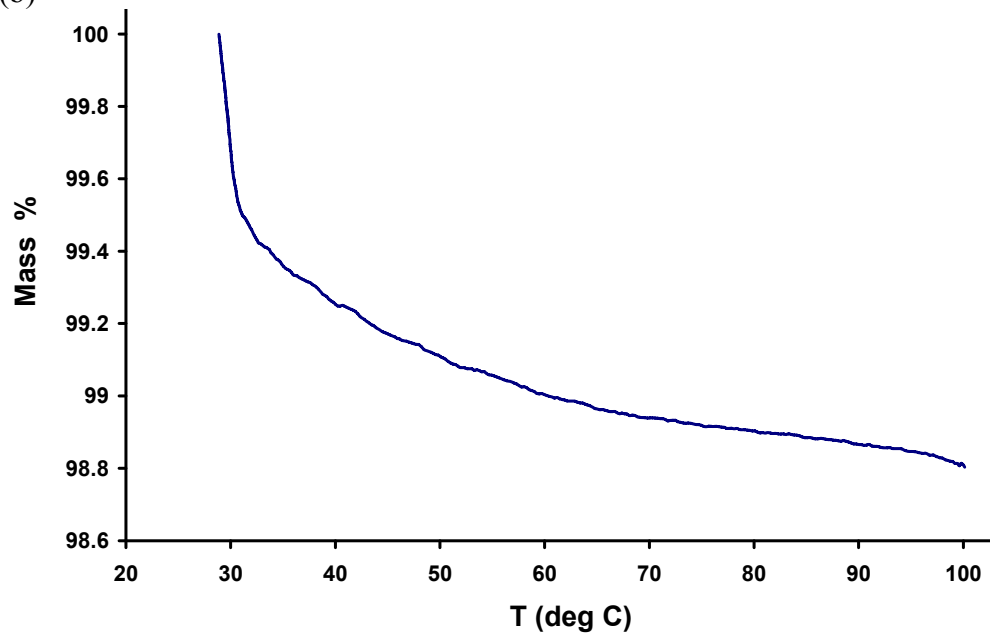

Figure S14. (a) Full TGA profile for **2** up to 700 °C. The first inflection point at 250 °C corresponds to a mass loss of 25%. (b) TGA data for **2** up to 100 °C only, showing a mass loss of 1.2% at this temperature. Based on the crystallographic formula $[Ni_3(BTB)_2(bipy)_3(EG)_3] \cdot$ (toluene), the calculated mass loss for the guest molecules and metal-bound EG is 15.5%. The TGA profiles clearly indicate that this mass is lost in the range 100 – 250 °C but does not occur as distinct mass losses, but is lost concomitantly resulting in framework degradation.

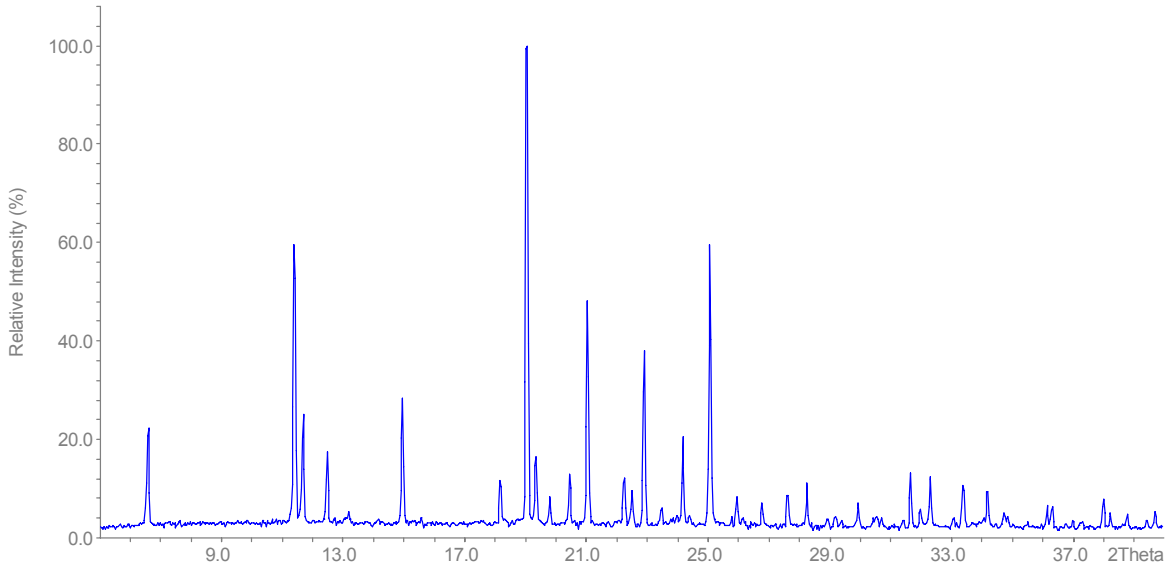

Figure S15. Powder X-ray diffraction data of a bulk sample of as-synthesised **2**. The sample was sealed in a glass capillary and measured in transmission mode on a Stoe-Stadi P diffractometer using Cu $K_{\alpha 1}$ radiation. Refined cell parameters: a = 31.2637(35) Å, c = 17.3266(48) Å, V = 14666.366(58) Å^3.

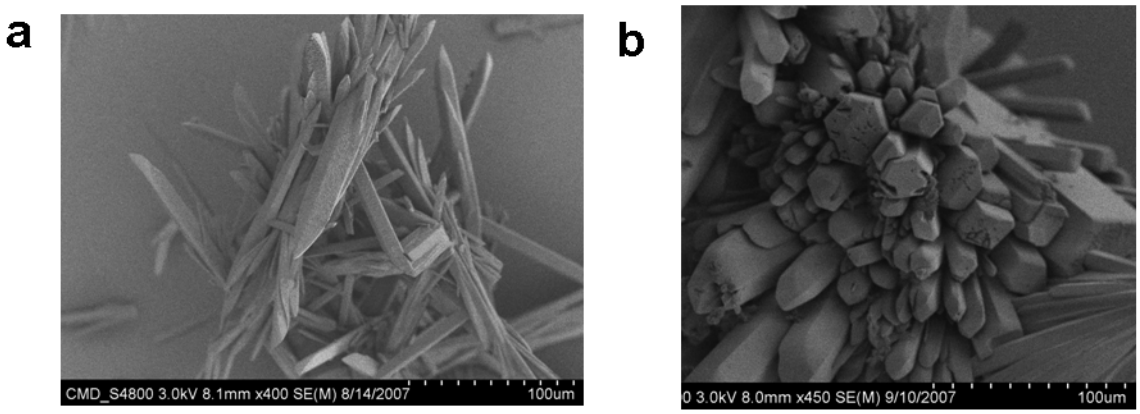

Figure S16. SEM images of crystalline samples of (a) framework **1** and (b) framework **2**. Note the change in crystal morphology from flat needles to blocks in the presence of toluene.